Published in final edited form as:
Biochemistry. 2013 October 22; 52(42): 7428–7438. doi:10.1021/bi401156a.

A substrate-assisted mechanism of nucleophile activation in a Ser-His-Asp containing C-C bond hydrolase

Antonio C. Ruzzini[†], **Shiva Bhowmik**[‡,⊥], **Subhangi Ghosh**[‡], **Katherine C. Yam**[†], **Jeffrey T. Bolin**[‡], and **Lindsay D. Eltis**[†,§,*]

[†]Department of Biochemistry & Molecular Biology, The University of British Columbia, Vancouver, BC, Canada

[§]Department of Microbiology & Immunology, The University of British Columbia, Vancouver, BC, Canada

[‡]Purdue Cancer Research Center and Markey Center for Structural Biology, Department of Biological Sciences, Purdue University, West Lafayette, IN, USA

Abstract

The *meta*-cleavage product (MCP) hydrolases utilize a Ser-His-Asp triad to hydrolyze a carbon-carbon bond. Hydrolysis of the MCP substrate has been proposed to proceed via an enol-to-keto tautomerization followed by a nucleophilic mechanism of catalysis. Ketonization involves an intermediate, ES^{red}, possessing a remarkable bathochromically-shifted absorption spectrum. We investigated the catalytic mechanism of the MCP hydrolases using DxnB2 from *Sphingomonas wittichii* RW1. Pre-steady-state kinetic and LC ESI/MS evaluation of the DxnB2-mediated hydrolysis of 2-hydroxy-6-oxo-6-phenylhexa-2,4-dienoic acid (HOPDA) to 2-hydroxy-2,4-pentadienoic acid (HPD) and benzoate support a nucleophilic mechanism catalysis. In DxnB2, the rate of ES^{red} decay and product formation showed a solvent kinetic isotope effect of 2.5 indicating that a proton transfer reaction, assigned here to substrate ketonization, limits the rate of acylation. For a series of substituted MCPs, this rate was linearly dependent on MCP pK_{a2} (β_{nuc} ~1). Structural characterization of DxnB2 S105A:MCP complexes revealed that the catalytic histidine is displaced upon substrate-binding. The results provide evidence for enzyme-catalyzed ketonization in which the catalytic His-Asp pair does not play an essential role. The data further suggest that ES^{red} represents a dianionic intermediate that acts as a general base to activate the serine nucleophile. This substrate-assisted mechanism of nucleophilic catalysis distinguishes MCP hydrolases from other serine hydrolases.

INTRODUCTION

The *meta*-cleavage product (MCP) hydrolases are involved in the aerobic catabolism of aromatic compounds by bacteria[(1)], hydrolyzing a C-C bond of MCPs produced from the extradiol ring cleavage of catechols. These α/β-hydrolase superfamily members possess the canonical elements of serine hydrolases including a Ser-His-Asp catalytic triad and an

[*]Corresponding Author: Lindsay D. Eltis – leltis@mail.ubc.ca/Tel: (604)-822-0042.
[⊥]**Present Addresses**
Department of Integrative Structural and Computational Biology, The Scripps Research Institute, 10550 North Torrey Pines Road, La Jolla, CA 92037.

Author Contributions
The manuscript was written through contributions of all authors. All authors have given approval to the final version of the manuscript.

Supporting Information. post-catalytic DxnB2:HPD spectra, H/D exchange, extended Brønsted analysis on k_{cat}/K_m, spectra of DxnB2:HOPDA complexes. This material is available free of charge via the Internet at http://pubs.acs.org.

'oxyanion hole'. However, studies on BphD, a biphenyl-degrading enzyme from *Burkholderia xenovorans* LB400 that hydrolyzes 2-hydroxy-6-oxo-6-phenylhexa-2,4-dienoic acid (HOPDA), have revealed a fundamental difference in how the catalytic machinery of MCP hydrolases functions. Thus, in the hydrolysis of HOPDA, acylation of BphD is independent of the catalytic histidine[2]. Interestingly, the esterase activity of BphD was histidine-dependent, suggesting alternative mechanisms for nucleophile activation and acylation in each of the C-C and C-O bond hydrolysis reactions[3]. More particularly, nucleophile activation appears to be catalyzed by the His-Asp pair for C-O bond cleavage, as in prototypical serine hydrolases. In contrast, a substrate-assisted nucleophilic mechanism of catalysis has been proposed for MCP hydrolysis[2] in which the electron-rich substrate acts as a general base (Scheme 1).

The difference in nucleophile activation for the acylation reaction in MCP and ester hydrolysis, respectively, highlights the profound effect of the distinct chemical nature of carbon-heteroatom (C-X, where X = N, O or S) and C-C bonds on their enzyme-catalyzed hydrolysis. Common obstacles to C-X and C-C bond hydrolysis include activation of the scissile bond and a water molecule, which are performed by a general acid and general base. The generally accepted mechanisms of α/β-hydrolases and serine proteases have been reviewed[4–6]. Of interest here is the identity of the atom in the leaving group, which contributes greatly to the chemical and kinetic mechanism of bond cleavage. The ability of the catalytic histidine to act as a general acid to protonate the leaving group during the collapse of the first tetrahedral oxyanion intermediate facilitates C-X bond cleavage. In contrast, carbon centers are typically non-basic, precluding the aforementioned role of the histidine as an acid, and necessitating an alternative electron sink for C-C cleavage.

The MCP hydrolases and at least two other enzyme families exploit a diketone or diketone-like functionality for C-C bond hydrolysis. First, the serine nucleophile-dependent and independent β-ketolases transform substrates that contain a β-diketone electron sink[7]. Another group of C-C bond hydrolases, exemplified by kynureninases, are cofactor-dependent, generating a β-ketiminium moiety using pyridoxal 5′-phosphate[8]. The MCP hydrolases are proposed to catalyze a substrate enol-to-keto tautomerization prior to C-C bond cleavage, generating an α,β-unsaturated δ-diketone[9]. Common to all these enzymatic reactions is the generation of an electron sink that is capable of stabilizing a leaving carbanion by charge delocalization. In contrast to each of these examples, mechanistic proposals for orotidine 5′-monophosphate decarboxylase invoke protonation during[10] or after[11] C-C bond fragmentation.

Two related aspects of the mechanism of MCP hydrolysis remain of high interest: the proposed substrate tautomerization and the nature of ES^{red}, an intermediate formed during the proposed tautomerization that is characterized by a bathochromically-shifted absorption spectrum[12]. With respect to tautomerization, generation of an α,β-unsaturated δ-diketone is dependent on protonation of the dienoate moiety at C5. Product analyses of reactions performed in $^{2}H_2O$ demonstrated that MhpC, the MCP hydrolase from the phenylpropionate catabolic pathway of *Escherichia coli*, catalyzed the stereospecific incorporation of deuterium into the H-5_E position of 2-hydroxy-2,4-pentadienoic acid (HPD)[13]. Stereospecific deuterium incorporation was also observed from ^{1}H NMR studies of the BphD-mediated hydrolysis of HOPDA[12]. Finally, the ability of BphD to catalyze the tautomerization of HPD to (*E*)-2-oxo-3-pentenoate was also cited as evidence for the electron-sink-generating enol-to-keto tautomerase activity[12, 14].

ES^{red} can be detected under single turnover conditions[12] and serine-to-alanine variants of MCP hydrolases trap a species whose visible spectrum resembles that of ES^{red}[14, 15]. The visible spectrum of the red-shifted intermediate is more consistent with a dianionic species.

Thus, the HOPDA dianion or enolate has a λ_{max} at 434 nm in solution whereas the monoanionic enol possesses a λ_{max} at 345 nm. Accordingly, these features argue for substrate ketonization involving protonation of a dianionic species, rather than the early proposal of an enol-to-keto tautomerization by the MCP hydrolases. A crystalline BphD S112A:HOPDA complex correlated ES^{red} to a non-planar dienoate-binding mode that included a *gauche*+ conformation about the C4–C5 bond[14]. Single crystal spectroscopy revealed that the observed, presumably productive, binding mode was remarkably similar to that of ES^{red} in solution. These structural studies represent the greatest insight into the nature of ES^{red} to date, and have revealed an astonishing suite of interactions between enzyme and substrate occurring within two specialized substrate-binding subsites. These polar (P-) and non-polar (NP-) subsites, named for their physicochemical properties, converge at the catalytic serine and oxyanion hole[12].

Due to the distinctive electronic absorption spectrum of ES^{red}, stopped-flow spectrophotometry has provided important insights into the mechanism of MCP hydrolases. The turnover of BphD is defined by three detectable steps: (i) ES^{red} formation, (ii) ES^{red} decay commensurate with formation of a species that absorbs at 270 nm, either the ketonized substrate or HPD[16], and (iii) deacylation, measured under steady-state conditions as k_{cat}. Step (ii) is typically only detected under single turnover conditions and both steps (ii) and (iii) have been used as indirect measures of acylation. However, the interpretation of the transients has been complicated by the half-site reactive BphD[2], a tetrameric enzyme. More specifically, ES^{red} decay is biphasic in BphD: both steps (ii) and (iii) are associated with the dissipation of a spectroscopic signal at ~490 nm. Furthermore, amplitude analysis of a stopped-flow experiment using a 2:1 BphD protomer-to-HOPDA ratio was initially used to suggest a two-conformation model of catalysis[12]. This model has been since supported by investigating the steady-state rate of HOPDA methanolysis by BphD, which is limited by half-site reactivity[3]. Interestingly, the hydrolysis of inhibitory polychlorinated biphenyl (PCB) metabolites by DxnB2, a dimeric MCP hydrolase from *Sphingomonas wittichii* RW1 that shares 23% amino acid sequence identity with BphD, was characterized by only two observable kinetic phases: (i) alternative ES complex formation and (ii) decay, which matched k_{cat}. This suggests that DxnB2 may be full-site reactive with respect to certain substrates[17] and may therefore be more amenable to transient state kinetic studies than BphD.

In this work, we investigated the MCP hydrolase catalytic mechanism using DxnB2. Reactions of DxnB2 and HOPDA were monitored using stopped-flow spectrophotometry. Solvent viscosity and isotope effects were measured to better define the kinetic and chemical mechanism. An extended Brønsted analysis using a series of HOPDA analogs was performed to relate substrate basicity to the reactivity of ES^{red}. Substrate binding modes correlated to ES^{red} were characterized in crystalline DxnB2 S105A:MCP binary complexes. The catalytic mechanism of the MCP hydrolases, specifically substrate and nucleophile activation, are discussed.

MATERIALS AND METHODS

Chemicals and reagents

All HOPDAs were produced according to published protocols[18] with the exception of 5,8-diF HOPDA (*vide infra*). The remaining chemicals were of analytical grade. DxnB2 WT and S105A were produced as previously described[17].

Preparation of 5,8-diF HOPDA

2′,6-diF Dihydroxybiphenyl (DHB) was generated from whole cell biotransformation of 2,2′-difluorobiphenyl using *Pandoraea pnomenusa* B-356 in the presence of 3-chlorocatechol. A 1 L culture of *P. pnomenusa* B-356 was grown on M9 + Goodies + 100 mg biphenyl until an $OD_{600\ nm}$ of 0.5. These cells were then harvested and washed three times with phosphate buffer saline (PBS, pH 7.3) to remove residual biphenyl. The harvested cells were divided into two flasks containing 500 mL PBS + 8 mg 2,2′-diF-biphenyl + 8 mg 3-chlorocatechol, an inhibitor of 2,3-DHB dioxygenase, the extradiol dioxygenase that produces MCPs. These flasks were then incubated at 30 °C for 90 min, shaking at 200 rpm. The two samples were pooled, acidified to pH 2.5, centrifuged and the supernatant was filtered to remove any insoluble 2,2′-difluorobiphenyl. The filtrate was extracted with three 200 mL volumes of ethyl acetate, dried with $MgSO_4$, and concentrated by rotary evaporation. Dry samples from each biotransformation were stored under nitrogen gas in an M. Braun Labmaster glovebox (Stratham, NH, USA) until further purification.

A Waters 2695 HPLC system (Waters Corp., Milford, MA) was used for the purification of DHBs. The dry samples were dissolved in a solution of 0.5% formic acid (v/v), 50% methanol (v/v). Residual precipitate was removed by centrifugation and filtration (0.45 μm). The mixtures were injected into a 250 × 10 mm Luna 5 μm C18(2) column (Phenomenex, Torrence, CA), equilibrated at a 50:50 ratio of eluents A and B, and operating at a flow rate of 3.5 mL/min. Eluent A was 0.5% formic acid (v/v) and B was methanol. Isocratic elution of 2′,6-diF-DHB was achieved after 25.5 min. Pure fractions were collected, pooled, and partially dried under a stream of N_2 gas to remove excess methanol, and the expected mass was confirmed using EI GC/MS.

The resulting solution containing fluorinated DHB was diluted in 200 mL of water and the pH was adjusted to 7.5 with 1 M NaOH prior to HOPDA preparation. HOPDAs were generated by enzymatic transformations of the corresponding DHB by 2,3-DHB dioxygenase[18]. 5,8-diF HOPDA, characterized as described for other MCPs[18], has an extinction coefficient $\varepsilon_{405\ nm} = 31.2\ mM^{-1}cm^{-1}$ (potassium phosphate buffer (I = 0.1 M), pH 7.5, 25 °C) and a pK_{a2} of 5.0 ± 0.2.

Steady-state kinetics

Steady-state kinetic parameters for DxnB2-catalyzed hydrolysis of 5,8-diF HOPDA were obtained by monitoring the decay of the enolate (A405 nm) in potassium phosphate buffer (I = 0.1M), pH 7.5 at 25 °C. All reactions were carried out in a 1 mL volume and the initial velocities were determined by a least squares linear fit to each individual progress curve within the Cary WinUV Software. Triplicate initial velocity measurements were plotted against substrate concentration (0.5 – 10 μM), and curve fitting was performed using dynamic weighting least-squares analysis in LEONORA[19].

Stopped-flow experiments

An SX.18MV stopped-flow reaction analyzer (Applied Photophysics Ltd., Leatherhead, UK) was used to perform transient-state kinetic measurements. The temperature of the optical cell and drive syringe chamber was maintained at 25 °C using circulating water. The concentration of reactants and specific buffer conditions are stated in the Results section as they depended on the aim of the specific experiment. In general, single turnover reactions were performed at either ~2:1 or 4:1 enzyme to substrate ratio whereas multiple turnover reactions were performed at 1 or 2.5 μM enzyme in the presence of 20 μM substrate. Multiple wavelength data were collected using the system's photodiode array (PDA) detector and Xe light source. A monochromator (4.96 nm/mm bandpass) open to 0.5 mm was employed to collect single wavelength data.

All reported values are derived from at least three replicates. Each replicate refers to an average of at least 5 shots from the stopped-flow syringes containing freshly prepared reactants. For each experiment the errors are reported as the standard deviation between replicates. The values were determined using the fitting options within the Applied Photophysics Pro-Data Software.

LC ESI/MS

The reaction of 4 μM DxnB2 and 20 μM HOPDA was allowed to age for 10 s before quenching with acetic acid 5% final (v/v). Samples were concentrated 10-fold and subject to LC ESI/MS as previously described for $BphD_{LB400}$[2]. The error reported for the MS data represents the standard deviation observed between three MS experiments. The fraction of acylated enzyme was estimated using the peak area of each of the three major observed species.

Crystallization, structure determination and refinement

Crystals of DxnB2 S105A were prepared as previously described[17]. Diffraction experiments were performed under cryogenic conditions (~100 K) at SER-CAT beamline 22-ID-D (for the S105A:5,8 diF-HOPDA complex) or BIO-CARS beamline 14-BM-C (for the S105A:HOPDA complex) at the Advanced Photon Source, Argonne National Laboratory, Argonne, IL, USA. Typical datasets included 200 to 300 frames at 0.5° intervals each exposed for 5–6 s at an X-ray wavelength of 1.0 Å. Software within the HKL2000 suite was utilized to process the images and scale and merge intensities[20].

Programs within the CCP4 program package[21] were employed to determine the structures of the DxnB2 S105A:HOPDA and DxnB2 S105A:5,8 diF-HOPDA complexes. Initial phases were obtained by molecular replacement using the structures of DxnB2 WT (for the S105A:5,8-diF HOPDA) or the DxnB2 S105A:3Cl-HOPDA complex (for the S105A:HOPDA complex) as search models. The search models were modified prior to use by removal of all water molecules, ligands and secondary conformations of residues. After obtaining the initial phases, rigid body refinement was followed by iterative cycles of atomic model refinement and model building performed using REFMAC[22] and COOT[23]. Substrates were manually built into the electron density using the molecular graphics programs O[24] and COOT or transformed from the coordinates of the BphD S112A:HOPDA complex[14]. Coordinates of the 5,8-diF HOPDA were generated by PRODRG[25]. The stereochemical properties of the models and hydrogen bonding were analyzed by programs PROCHECK[26] and REDUCE[27].

Electronic absorption spectroscopy

Electronic absorption spectra of HOPDAs alone or in complexes with the DxnB2 S105A variant were recorded using a Cary5000 spectrophotometer equipped with a thermostatted cuvette holder that was maintained at 25 °C. Each enzyme-substrate (ES) complex was formed by mixing 40 μM DxnB2 S105A with 10 μM substrate in potassium phosphate buffer (I = 0.1 M), pH 7.5. The half-life of the DxnB2 S105A:HOPDA complex was determined by measuring spectra of three samples at 20 min intervals over 20 hours, and a single exponential equation was fit to the observed decay.

Absorption spectra of the crystalline DxnB2 S105A:HOPDA complex were obtained at 100 K before and after X-ray exposure and diffraction measurements using an online 4DX microspectrophotometer (4DX-ray Systems AB, Uppsala, Sweden) at BIO-CARS beamline 14-BM-C. The spectrum of the light source and that of the mount solution (obtained by passing light through the loop at a position avoiding the protein crystal) have been subtracted from the reported spectrum.

Low-temperature measurements were performed using Cary6000I spectrophotometer (Agilent) equipped with a closed-cycle Omniplex OM-8 He cryostat (ARS Inc., Macungi, PA). A sample consisting of 2 mM DxnB2 S105A and 1 mM HOPDA was mixed with an equal volume of glycerol before being deposited between two quartz windows separated by a polycarbonate spacer (~25 μm). The assembly was mounted on a sample rod and frozen rapidly to ~10 K. Data were collected at a 0.6 nm bandwidth between 1000 and 200 nm. A background correction was performed manually using Origin 8.0 (OriginLab Corporation, Northampton, MA), and the spectrum is reported between 600 and 300 nm.

RESULTS

A pre-steady-state kinetic burst of HPD formation

Mechanistic investigation of the MCP hydrolases has focused on tetrameric homologs that show half-site reactivity. Since DxnB2 is dimeric and was full-site reactive with 3-Cl HOPDA, we began our investigation by probing the enzyme's pre-steady-state kinetic behavior using stopped-flow spectrophotometry. The hydrolysis of 20 μM HOPDA or 9-Cl HOPDA by 1 and/or 2.5 μM DxnB2 was measured in potassium phosphate buffer (I = 0.1 M), pH 7.5 at 25 °C. These two substrates were selected on the basis of distinct steady-state kinetic behavior: k_{cat} values measured for the DxnB2-mediated hydrolysis of HOPDA and all other tested monochlorinated substrates ranged between 0.25 and 0.88 s^{-1} whereas k_{cat} was 5.1 s^{-1} for 9-Cl HOPDA[28]. Reactions were monitored at 270 nm to follow the progress of HPD formation[16] (Figure 1), and the values derived from fitting the stopped-flow measurements to a burst equation are summarized in Table 1. For HOPDA, a pre-steady-state burst occurred with a rate constant of ~62 s^{-1}. Quantification of the amount of HPD produced during each burst phase indicated that hydrolysis was a full-site event, suggesting that half-site reactivity may not be a universal feature of the MCP hydrolases. The observed steady-state rate constant for the subsequent hydrolysis (k_{ss}) was ~0.4 s^{-1}, similar to the previously reported k_{cat} ~0.47 s^{-1} for the hydrolysis of HOPDA[28].

In contrast to HOPDA, quantification of HPD formed during the burst from the first turnover of 9-Cl HOPDA indicated that only ~67% of the enzyme was reactive. The measured pre-steady-state rate constant for HPD formation was ~3.5-fold slower for 9-Cl HOPDA than for HOPDA and the k_{ss} ~4.3 s^{-1} was similar to the reported k_{cat} value. Although half-site reactivity has been reported for BphD, the mechanism underlying less-than-full-sites burst for 9-Cl HOPDA is unclear. The observed kinetic behavior more closely resembles the reaction of BphD and *p*-nitrophenyl benzoate in which ~70% reactivity was modeled[3]. In spite of the unexplained nature of the burst of HPD from the hydrolysis of 9-Cl HOPDA, the observation of pre-steady-state bursts from both HOPDA and 9-Cl HOPDA is consistent with a proposal that DxnB2 utilizes a covalent mechanism of catalysis.

Evidence for an acyl-enzyme intermediate in DxnB2 by LC ESI/MS

To more confidently assign a nucleophilic mechanism of catalysis to DxnB2, chemical quench experiments were carried out, and intact enzyme samples were analyzed by LC ESI/MS. Reactions of 4 μM DxnB2 and 20 μM HOPDA were aged for 10 s before quenching with a final volume of 5% acetic acid (v/v). LC ESI/MS analyses of the reaction mixture revealed acylation of ~85% of the DxnB2 sample (Figure 2). The observed mass of DxnB2 was 30198 ± 7 Da (~220 ppm) was within error of the predicted mass of 30194 Da. Upon reaction with HOPDA, two additional signals were observed at M+104 and M+324. Both signals were interpreted as a benzoylated species with the second representing an acyl-enzyme in complex with an additional substrate molecule. The observation of additional non-covalent binding is consistent with the K_{si} of ~36 μM reported for the steady-state turnover of HOPDA by DxnB2[28]. Moreover, an additional substrate molecule was

observed in the crystalline BphD H265Q acyl-enzyme[2]. Overall, the fraction of acylated enzyme observed was significantly greater than the ~45% detected in BphD[2], reflecting full rather than half-site reactivity of DxnB2 toward HOPDA.

A solvent kinetic isotope effect on ES^{red} decay

The apparent full-site turnover of DxnB2 afforded further evaluation of the kinetic mechanism. Single turnover experiments were initially performed by stopped-flow using 16 μM DxnB2 and 4 μM HOPDA in potassium phosphate buffer (I = 0.1 M), pH 7.5 at 25 °C. ES^{red} formation was characterized by a 53 nm bathochromic-shift of the substrate's absorption spectrum that occurred within the dead-time of the stopped-flow apparatus ($1/\tau_1 > 500\ s^{-1}$; Figure 3A). Its decay at 487 nm and formation of the species absorbing at 270 nm both proceeded with rate constants of ~69 s^{-1} ($1/\tau_2$; Figure 3B). This step was insensitive to the addition of viscogens to the reaction media, either 30% sucrose (w/v) or 30% glycerol (v/v), and identical rate constants were measured at ~2:1 ratio of DxnB2 to HOPDA (Table 2), indicating that the observed events are intramolecular. Following the hydrolysis of HOPDA, a spectral feature attributed to HPD rebinding and decay was also observed in the visible region, accounting for ~1% of the total change in amplitude (Figure S1). Likewise, the ketonization of HPD was also detectable at 270 nm (Figure 3B), a post-catalytic event that was previously reported for $BphD_{LB400}$[12]. Again, DxnB2 revealed no trace of half-site reactivity with respect to the hydrolysis of HOPDA, and the observed event was ~150-fold faster than k_{cat}, consistent with a mechanism in which deacylation is rate-limiting.

The reactivity of ES^{red} was further probed by measuring a solvent kinetic isotope effect (SKIE). Stopped-flow was used to monitored reactions of 8.2 μM DxnB2 and 4 μM HOPDA in a 95% (v/v) deuterated potassium phosphate buffer (I = 0.1 M, pD 7.5; Figure 4). Reactants were incubated for 2 hours prior to reaction to allow uniform H/D exchange into the substrate (Figure S2) and catalytically relevant residues. Two equivalents of deuterium were incorporated into ~63% of the sample. This exchange was previously detected at positions H-3 and H-5 of 2-hydroxy-6-keto-nona-2,4-diene 1,9-dioic acid[9] and HOPDA[12] by ^{1}H NMR. Deuteration of the substrate at these positions is not suspected to significantly perturb the kinetics of the reaction. Theoretically, an inverse α-secondary deuterium KIE would be expected for the transition of the fully conjugated substrate (C5 sp^2) to the (3*E*)-2,6-dioxo-6-phenylhexa-3-enoic acid (C5 sp^3) during substrate activation. Interestingly, reaction measurements in the deuterated buffer revealed an SKIE of 2.5 for $1/\tau_2$, which slowed to ~28 s^{-1} (Figure 4 and Table 2). This significant SKIE on $1/\tau_2$ indicates a rate-determining proton transfer, ultimately affording the explicit assignment of this transient kinetic phase to substrate ketonization. As expected, the rate of acylation and HPD formation is limited by substrate activation to generate an electron sink that can support bond cleavage.

An extended Brønsted analysis of substrate tautomerization

To further explore this ketonization reaction, we examined single turnover reactions for DxnB2 with a series of substituted HOPDAs. Specifically, 4 μM of each substrate, including 5-Cl, 8-Cl, 9-Cl and 5,8-diF HOPDA, was hydrolyzed by 16 μM DxnB2 in potassium phosphate buffer (I = 0.1 M) pH 7.5 at 25 °C (Figure 5 and Table 3). Each reaction proceeded through an intermediate characterized by a red-shifted absorption spectrum for which λ_{max} ranged between ~470 and 490 nm. In line with the 67% pre-steady-state kinetic burst of HPD formation observed during the reaction of DxnB2 and 9-Cl HOPDA, the presence of a phenyl ring-substituent altered the number of observable steps during a single DxnB2 turnover. In particular, an additional transient step suggested non-equivalence among DxnB2 active sites.

As described for HOPDA and 3-Cl HOPDA[29], two detectable transient kinetic steps were observed during the single turnover of 5-Cl HOPDA. First, ES^{red} formation occurred with a slower and thus measurable rate constant of ~310 s^{-1}, and the intermediate was characterized by a λ_{max} at 472 nm. The subsequent ketonization of 5-Cl HOPDA, measured at both 472 and 270 nm, proceeded with a rate constant of ~2.8 s^{-1}. In contrast to HOPDA and 5-Cl HOPDA, the DxnB2-mediated cleavage of 5,8 diF-HOPDA occurred with three detectable steps. Specifically, upon ES^{red} formation, $1/\tau_1$ ~500 s^{-1} at 485 nm, an additional spectral change was observed prior to ketonization. A small decrease in the signal at 485 nm, accounting for only 2.3% of the total change in amplitude, suggested that the two initial processes correspond to 5,8-diF HOPDA destabilization. The final observable phase, $1/\tau_3$ ~0.13 s^{-1}, was also detected at 270 nm and matched the k_{cat} value, which was determined independently by monitoring enolate decay at 405 nm (k_{cat} = 0.13 ± 0.01 s^{-1}, k_{cat}/K_m = 9.4 ± 0.8 10^4 $M^{-1}s^{-1}$, K_m = 1.3 ± 0.1). Remarkably, ketonization rather than deacylation represented the rate-limiting step of the DxnB2-catalyzed hydrolysis of 5,8 diF-HOPDA.

Three steps were also detected during the turnover of 8-Cl and 9-Cl HOPDA, including the biphasic decay of ES^{red} commensurate with production of a species absorbing at 270 nm. The results are reminiscent of the two distinct acylation events proposed for the half-site reactive $BphD_{LB400}$[12]. However, the SKIE reported for HOPDA indicate that the initial phase of ES^{red} decay is limited by ketonization whereas the processes governing the non-equivalent active site behavior are unknown. Thus, DxnB2 catalyzed the ketonization of 8-Cl and 9-Cl HOPDA with rate constants of 4.3 and 20 s^{-1}, respectively. For 8-Cl HOPDA ketonization at the second active site, $1/\tau_3$ ~1 s^{-1}, could be distinguished from the rate-limiting enzyme deacylation, occurring at 0.48 s^{-1} [28]. In contrast, $1/\tau_3$ ~7 s^{-1} was within error of the k_{cat} measured for 9-Cl HOPDA, suggesting that ketonization may be rate-limiting even for more basic substrates. The assignment of $1/\tau_3$ to substrate ketonization was supported by the lack of a viscosity effect for the reaction of DxnB2 and 9-Cl HOPDA in the presence of 30% sucrose (w/v).

Regardless of the basis of less than full-sites reactivity, an extended Brønsted plot of the observed rate constants for ketonization, $\log(1/\tau_2)$, versus the pK_{a2} value of each substrate demonstrated a positive linear correlation (R^2 = 0.97) and β_{nuc} = 1.17 ± 0.06 (Figure 6). A similar analysis of the DxnB2 specificity constants also revealed a β_{nuc} ~1 (Figure S3). These results establish that the reactivity of the substrates towards protonation at C5 reflects their enol:enolate equilibrium in solution.

Characterization of crystalline ES complexes

As previously reported for other MCP hydrolase catalytic serine-to-alanine variants, DxnB2 S105A stabilized a species that resembled ES^{red} (Figure S4). In solution the half-life of the DxnB2 S105A:HOPDA complex was 6.2 ± 0.1 hours whereas the stability of S105A:5,8-diF HOPDA appeared to match that of the enzyme sample as precipitation and loss of the orange-color were concurrent and not readily apparent until several days of incubation at room temperature. To further probe the nature of ES^{red} in DxnB2, crystals of DxnB2 S105A were incubated with either HOPDA or 5,8-diF HOPDA prior to diffraction experiments (Table 4), which yielded structural results similar to those reported for BphD[14] and HsaD[15], a tetrameric homologue from *Mycobacterium tuberculosis*. For example, polar contacts between the conserved P-subsite residues, Gly35, Asn43, Asn104, Arg180 and Trp256 were observed between the enzyme and the MCP dienoate moiety.

The S105A:HOPDA and S105A:5,8-diF HOPDA binary complexes were refined to 2.3 Å and 2.2 Å with the substrate modeled at 80% and 100% occupancy, respectively. The lid domain of the DxnB2 models differed markedly from previously reported structures[17]. The first difference was observed in the NC-loop, originally defined as a variable protein

segment that connects the α/β-hydrolase core through β6 to the N-terminus of the lid domain in the epoxide hydrolases[30]. Specifically, the NC-loop was helical in the two binary complexes reported here. Next, the N-terminal helix α5 of the lid domain was well-ordered and defined by both electron density maps. These differences are reflected by a large number of enzyme-substrate contacts similar to those reported in BphD[12, 14]. The resolution of the diffraction data and the unbiased electron density maps did not permit reliable, independent attempts to define the conformation of each substrate at the DxnB2 S105A active site. Ultimately, the HOPDA molecules were refined as a (3*E*)-2,6-dioxo-6-phenylhexa-3-enoic acid based on the observed binding mode and single crystal spectrum of a 1.6 Å BphD S112A:HOPDA complex[14]. However, an (3*E*, 5*E*)-2-oxo-6-oxido-6-phenylhexa-3,5-dienoaic acid could also be modeled into the electron density.

In the crystalline DxnB2 S105A:HOPDA binary complex, a non-planar dienoate-binding mode that includes a *cis*-conformation about the C4–C5 bond (Figure 7A–B) was correlated to ES^{red} by single crystal spectroscopy (Figure 8). The electronic absorption of the crystalline complex prior to and following X-ray exposure resembled that measured in solution or frozen as a glass in 50% glycerol at ~10 K. The λ_{max} values of the most bathchromically-shifted signal in all three spectra were within 10 nm of each other: $\lambda_{max\ crystal}$ ~502 nm, $\lambda_{max\ solution}$ ~500 nm, $\lambda_{max\ 10K}$ ~510 nm. The results also indicate that the crystalline ES^{red} is not destroyed or significantly altered during data collection. Interestingly, the resolution of the 10 K spectra revealed the underlying complexity of the ES^{red} spectrum, suggesting at least 6 distinct electronic transitions contribute to the spectrum observed in solution or in the crystalline state.

Comparison of the DxnB2 S105A:HOPDA or 5,8-diF HOPDA binary complexes to substrate-free DxnB2 structures[17] revealed that productive substrate-binding, defined here as orange-colored crystals, was accompanied by a coordinated displacement of His255 and Trp256 from residue 105. Instead of H-bonding with Ser105, a polar interaction between His255 and Asn104 is evident in the MCP-bound structures (Figure 7C). Thus, during catalysis by the wild-type enzyme, the Ser105 side-chain would be free to react with a carbanionic MCP intermediate to complete both substrate ketonization and enzyme nucleophile activation. Together with the kinetic analyses, this structural data suggest a non-essential role for the His-Asp pair in serinate formation.

DISCUSSION

The investigation of DxnB2 presented herein provides a more detailed understanding of the catalytic mechanism of the MCP hydrolases. The observation of a pre-steady-state kinetic burst and a covalently modified enzyme sample consistent with a benzoylation (M+104) represent the second account of a nucleophilic mechanism by an MCP hydrolase. These additional results extend the observation of an acyl-enzyme in BphD[2] to a full-site reactive MCP hydrolase, further establishing that these enzymes do not use a general base mechanism as had been previously proposed[31]. Moreover, this is the first mechanistic study of a dimeric MCP hydrolase, and the differences between the reactivity of DxnB2 and other tetrameric MCP hydrolases revealed novel insight into the early steps of catalysis.

The full-site reactivity of DxnB2 towards HOPDA afforded a more detailed investigation of the catalytic steps preceding C-C bond cleavage in MCP hydrolases. Prior to this study, the interpretation of kinetic data associated with HOPDA turnover was complicated by half-site reactivity. As an example, viscosity effects were reported on $1/\tau_1$ and $1/\tau_2$ but not $1/\tau_3$ ($\sim k_{cat}$) for the BphD-mediated hydrolysis of HOPDA under single turnover conditions[12]. In DxnB2, the rate constants for ES^{red} formation, $1/\tau_1$, exceeded 500 s^{-1} and were not detectably slowed by the addition of a viscogen during turnover of HOPDA and 9-Cl

HOPDA. The viscosity effects reported on $1/\tau_1$ for BphD and DxnB2 during turnover of 3-Cl HOPDAs have been used to assign the first detectable step to a bimolecular event[12, 29]. In contrast, the origin of the viscosity effect on $1/\tau_2$ for the reaction of BphD and HOPDA is unclear but may be linked to half-site reactivity. In the two-conformation model, for example, a tetramer-specific enzyme conformational change, slowed by the addition of a viscogen, may contribute to the rate of acylation ($1/\tau_2$). For DxnB2 and HOPDA, the lack of a viscosity effect on $1/\tau_2$ and the monophasic decay of ES^{red} measured for the reaction suggest that this step represents ketonization or acylation.

By establishing that the decay of ES^{red} involves a proton transfer, the observation of an SKIE on the decay of the visible absorbance signal at 487 nm provides evidence that this intermediate represents a dianionic species and that its decay represents its ketonization. An intriguing possibility is that the catalytic serine protonates the MCP dianion at C5: the Ser105 hydroxyl readily exchanges with the solvent[32] and therefore the SKIE may reflect transfer from an O-D group. In the substrate-assisted mechanism depicted in Scheme 1, the first step involves a conformational equilibrium that raises the pK_{a2} of the incipient HOPDA dianion. Although ES^{red} is a dianionic intermediate, the cause of the spectral perturbations and the electronic nature of this intermediate remain unknown. The carbanionic intermediate in Scheme 1 reflects the position that is protonated and its pK_{a2} should be compatible with the proposed proton transfer from the Ser105 hydroxyl to C5. While carbanions are typically associated with high pK_a values, the MCP's conjugated system of electrons likely has a stabilizing effect. Importantly, this mechanism of ketonization would account for the His-independent nucleophile activation in MCP hydrolysis[2]. That substrate ketonization determines the rate of acylation further highlights the importance of generating an electron sink for the C-C bond cleavage reaction. While the stereochemical course of protonation of the pro-*S* position of C5 has been inferred from NMR studies of deuterium incorporation[9, 12, 13], this is the first definitive report on the rate of MCP ketonization. The ability to definitively assign $1/\tau_2$ to substrate ketonization allowed additional studies of the process.

The relationship between substrate basicity and the rate of ketonization supports the proposed role of the substrate acting as a general base for nucleophile activation. Indeed, the detection of a substituent effect indicates that nucleophile activation and attack of the serinate on the carbonyl are not concerted. Thus, proton transfer to C5 ultimately determines the apparent rate constant for acylation, with nucleophilic attack occurring faster than >70 s^{-1}. The acylation reaction is characterized by both ES^{red} decay and the concomitant production of a species that absorbs at 270 nm, which has been assigned to HPD[16]. The measured β_{nuc} value of ~1 reflects the expected change in charge upon protonation of ES^{red}, echoing the measured SKIE. White and Jencks interpreted a similar substituent effect for the reaction of succinyl-CoA:3-ketoacid CoA transferase as a change in charge from −1 to 0 at the transition state[33]. In the MCP hydrolases, the correlation reflects the conversion of a dianionic intermediate to an α/β-unsaturated δ-diketone carboxylate. Overall, the measured β_{nuc} and SKIE provide empirical evidence for a proton transfer to C5 that precedes nucleophilic attack by the MCP hydrolases.

Although substrate ketonization limits the rate of acylation, deacylation is typically the rate-determining step in catalysis, occurring between 0.4 and 5 s^{-1}. Rate-limiting ketonization was observed for two substrates: 9-Cl and 5,8-diF HOPDA. In the former case, the ketonization of 9-Cl HOPDA limited the turnover of only a fraction of active sites. That is, the substrate elicited non-equivalence of the active sites in a manner that is somewhat reminiscent of the two-conformation model associated with the half-site reactive BphD[2, 12]. Beyond the apparent dependence on a phenyl-ring substituent, the molecular

basis of the less-than-full-site reactivity of DxnB2 is puzzling but merits further investigation considering the environmental relevance of ring-substituted PCB metabolites.

The ability of electron-withdrawing substituents to stabilize the dianionic ES^{red} intermediate was most prominent for turnover of 5,8-diF HOPDA. For this reaction, steady-state turnover was limited by the rate of ketonization demonstrated by the agreement of $1/\tau_2$ and k_{cat} values of ~0.13 s^{-1}. While the precise electronic nature of ES^{red} remains unknown, the proton transfer event suggests that accumulation of negative charge at C5 is required. The strong inductive effect of a F-substituent at the reaction center is likely to stabilize the requisite, reactive carbanionic intermediate, and the electronic absorption spectrum of ES^{red} is consistent with that of a carbanionic species.

Overall, the reported SKIE and β_{nuc} support the substrate-assisted mechanism of catalysis proposed for the MCP hydrolases. Furthermore, the data implicate ES^{red} as a doubly charged species. Indeed, the MCP hydrolases represent a remarkable example of divergent evolution of the Ser-His-Asp catalytic triad. Despite the capacity of the triad to effect C-O bond cleavage using the canonical ‘charge-relay’ system[(3)], the enzyme appears to utilize charge on the MCP substrate postponing the direct involvement of the His-Asp dyad until the deacylation reaction.

Supplementary Material

Refer to Web version on PubMed Central for supplementary material.

Acknowledgments

Funding Sources

This work supported by a Discovery grant from the Natural Sciences and Engineering Research Council (NSERC) of Canada to L.D.E. and an NSERC PGS to A.C.R. Use of the APS was supported by US DOE under contract No, W-31-109-Eng-38. SER-CAT funding may be found at www.ser-cat.org/members.html and BioCARS Sector 12 was supported by NCRR (RR007707) and NIGMS (P41GM103543) grants from the NIH.

Drs. Grant Mauk and Federico Rosell helped collect visible absorbance spectra under cryogenic conditions. Dr. Vukica Srajer assisted with the single crystal spectroscopy. Dr. Jiyuan Ke initiated the crystallographic studies.

ABBREVIATIONS

HOPDA	2-hydroxy-6-oxo-6-phenylhexa-2,4-dienoic acid
HPD	2-hydroxy-2,4-pentadienoic acid
MCP	*meta*-cleavage product
SKIE	solvent kinetic isotope effect

References

1. Bayly RC, di Berardino D. Purification and properties of 2-hydroxy-6-oxo-2,4-heptadienoate hydrolase from two strains of Pseudomonas putida. J Bacteriol. 1978; 134:30–37. [PubMed: 77272]
2. Ruzzini AC, Ghosh S, Horsman GP, Foster LJ, Bolin JT, Eltis LD. Identification of an acyl-enzyme intermediate in a meta-cleavage product hydrolase reveals the versatility of the catalytic triad. J Am Chem Soc. 2012; 134:4615–4624. [PubMed: 22339283]
3. Ruzzini AC, Horsman GP, Eltis LD. The catalytic serine of meta-cleavage product hydrolases is activated differently for C-O bond cleavage than for C-C bond cleavage. Biochemistry. 2012; 51:5831–5840. [PubMed: 22747426]

4. Holmquist M. Alpha/Beta-hydrolase fold enzymes: structures, functions and mechanisms. Curr Protein Pept Sci. 2000; 1:209–235. [PubMed: 12369917]
5. Bornscheuer UT, Kazlauskas RJ. Catalytic promiscuity in biocatalysis: using old enzymes to form new bonds and follow new pathways. Angew Chem Int Ed Engl. 2004; 43:6032–6040. [PubMed: 15523680]
6. Hedstrom L. Serine protease mechanism and specificity. Chem Rev. 2002; 102:4501–4524. [PubMed: 12475199]
7. Grogan G. Emergent mechanistic diversity of enzyme-catalysed beta-diketone cleavage. Biochem J. 2005; 388:721–730. [PubMed: 15934927]
8. Phillips RS. Structure, mechanism, and substrate specificity of kynureninase. Biochim Biophys Acta. 2011; 1814:1481–1488. [PubMed: 21167323]
9. Lam WW, Bugg TD. Purification, characterization, and stereochemical analysis of a C-C hydrolase: 2-hydroxy-6-keto-nona-2,4-diene-1,9-dioic acid 5,6-hydrolase. Biochemistry. 1997; 36:12242–12251. [PubMed: 9315862]
10. Begley TP, Ealick SE. Enzymatic reactions involving novel mechanisms of carbanion stabilization. Curr Opin Chem Biol. 2004; 8:508–515. [PubMed: 15450493]
11. Van Vleet JL, Reinhardt LA, Miller BG, Sievers A, Cleland WW. Carbon isotope effect study on orotidine 5′-monophosphate decarboxylase: support for an anionic intermediate. Biochemistry. 2008; 47:798–803. [PubMed: 18081312]
12. Horsman GP, Ke J, Dai S, Seah SY, Bolin JT, Eltis LD. Kinetic and structural insight into the mechanism of BphD, a C-C bond hydrolase from the biphenyl degradation pathway. Biochemistry. 2006; 45:11071–11086. [PubMed: 16964968]
13. Li JJ, Bugg TD. Stereochemistry of the reaction catalysed by 2-hydroxy-6-keto-6-phenyl-hexa-2,4-dienoic acid 5,6-hydrolase (BphD). Chem Commun (Camb). 2005:130–132. [PubMed: 15614396]
14. Horsman GP, Bhowmik S, Seah SY, Kumar P, Bolin JT, Eltis LD. The tautomeric half-reaction of BphD, a C-C bond hydrolase. Kinetic and structural evidence supporting a key role for histidine 265 of the catalytic triad. J Biol Chem. 2007; 282:19894–19904. [PubMed: 17442675]
15. Lack NA, Yam KC, Lowe ED, Horsman GP, Owen RL, Sim E, Eltis LD. Characterization of a carbon-carbon hydrolase from Mycobacterium tuberculosis involved in cholesterol metabolism. J Biol Chem. 2010; 285:434–443. [PubMed: 19875455]
16. Pollard JR, Henderson IMJ, Bugg TDH. Chemical and biochemical properties of 2-hydroxypentadienoic acid, a homologue of enolpyruvic acid. Chem Commun. 1997:1885–1886.
17. Ruzzini AC, Bhowmik S, Yam KC, Ghosh S, Bolin JT, Eltis LD. The Lid Domain of the MCP Hydrolase DxnB2 Contributes to the Reactivity toward Recalcitrant PCB Metabolites. Biochemistry. 2013; 52:5685–5695. [PubMed: 23879719]
18. Seah SY, Labbe G, Nerdinger S, Johnson MR, Snieckus V, Eltis LD. Identification of a serine hydrolase as a key determinant in the microbial degradation of polychlorinated biphenyls. J Biol Chem. 2000; 275:15701–15708. [PubMed: 10821847]
19. Cornish-Bowden, A. Analysis of Enzyme Kinetic Data. Oxford University Press; New York: 1995.
20. Otwinowski, Z.; Minor, W. Methods in Enzymology. Academic Press; New York: 1997. Processing of X-ray Diffraction Data Collected in Oscillation Mode, In; p. 307-326.
21. Winn MD, Ballard CC, Cowtan KD, Dodson EJ, Emsley P, Evans PR, Keegan RM, Krissinel EB, Leslie AG, McCoy A, McNicholas SJ, Murshudov GN, Pannu NS, Potterton EA, Powell HR, Read RJ, Vagin A, Wilson KS. Overview of the CCP4 suite and current developments. Acta Crystallogr D Biol Crystallogr. 2011; 67:235–242. [PubMed: 21460441]
22. Murshudov GN, Vagin AA, Dodson EJ. Refinement of macromolecular structures by the maximum-likelihood method. Acta Crystallogr D Biol Crystallogr. 1997; 53:240–255. [PubMed: 15299926]
23. Emsley P, Cowtan K. Coot: model-building tools for molecular graphics. Acta Crystallogr D Biol Crystallogr. 2004; 60:2126–2132. [PubMed: 15572765]
24. Jones TA, Zou JY, Cowan SW, Kjeldgaard M. Improved methods for building protein models in electron density maps and the location of errors in these models. Acta Crystallogr A. 1991; 47(Pt 2):110–119. [PubMed: 2025413]

25. Schuttelkopf AW, van Aalten DM. PRODRG: a tool for high-throughput crystallography of protein-ligand complexes. Acta Crystallogr D Biol Crystallogr. 2004; 60:1355–1363. [PubMed: 15272157]

26. Laskowski RA, MacArthur MW, Moss D, Thornton JM. PROCHECK: a program to check the stereochemical quality of protein structures. J Appl Crystallogr. 1993; 26:283–291.

27. Word JM, Lovell SC, Richardson JS, Richardson DC. Asparagine and glutamine: using hydrogen atom contacts in the choice of side-chain amide orientation. J Mol Biol. 1999; 285:1735–1747. [PubMed: 9917408]

28. Seah SY, Ke J, Denis G, Horsman GP, Fortin PD, Whiting CJ, Eltis LD. Characterization of a C-C bond hydrolase from Sphingomonas wittichii RW1 with novel specificities towards polychlorinated biphenyl metabolites. J Bacteriol. 2007; 189:4038–4045. [PubMed: 17416660]

29. Ruzzini, AC.; Bhowmik, S.; Ghosh, S.; Bolin, JT.; Eltis, LD. The lid domain of the MCP hydrolase DxnB2 contributes to an increased specificity for recalcitrant PCB metabolites. 2013.

30. Barth S, Fischer M, Schmid RD, Pleiss J. Sequence and structure of epoxide hydrolases: a systematic analysis. Proteins. 2004; 55:846–855. [PubMed: 15146483]

31. Bugg TD, Fleming SM, Robertson TA, Langley GJ. 2-hydroxy-6-keto-nona-2,4-diene 1,9-dioic acid 5,6-hydrolase: evidence from 18O isotope exchange for gem-diol intermediate. Methods Enzymol. 2002; 354:106–118. [PubMed: 12418219]

32. Liepinsh E, Otting G, Wuthrich K. NMR spectroscopy of hydroxyl protons in aqueous solutions of peptides and proteins. J Biomol NMR. 1992; 2:447–465. [PubMed: 1384851]

33. White H, Jencks WP. Mechanism and specificity of succinyl-CoA:3-ketoacid coenzyme A transferase. J Biol Chem. 1976; 251:1688–1699. [PubMed: 1254594]

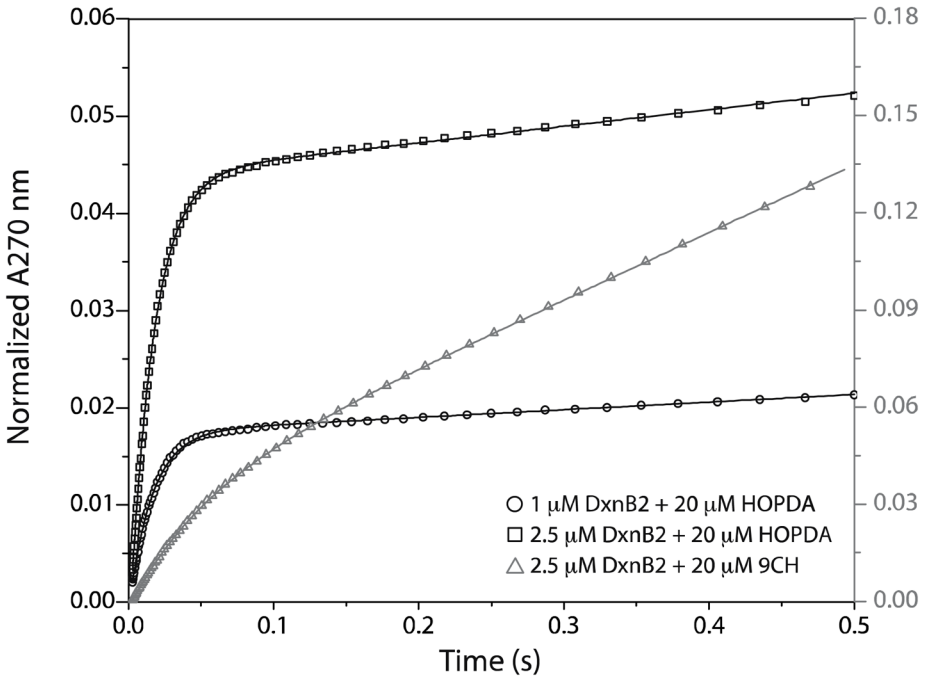

Figure 1.

Results from representative stopped-flow experiments demonstrating the pre-steady-state kinetic burst of HPD formation from HOPDA (black) and 9 Cl-HOPDA (grey) by DxnB2. For clarity, not all data points are shown.

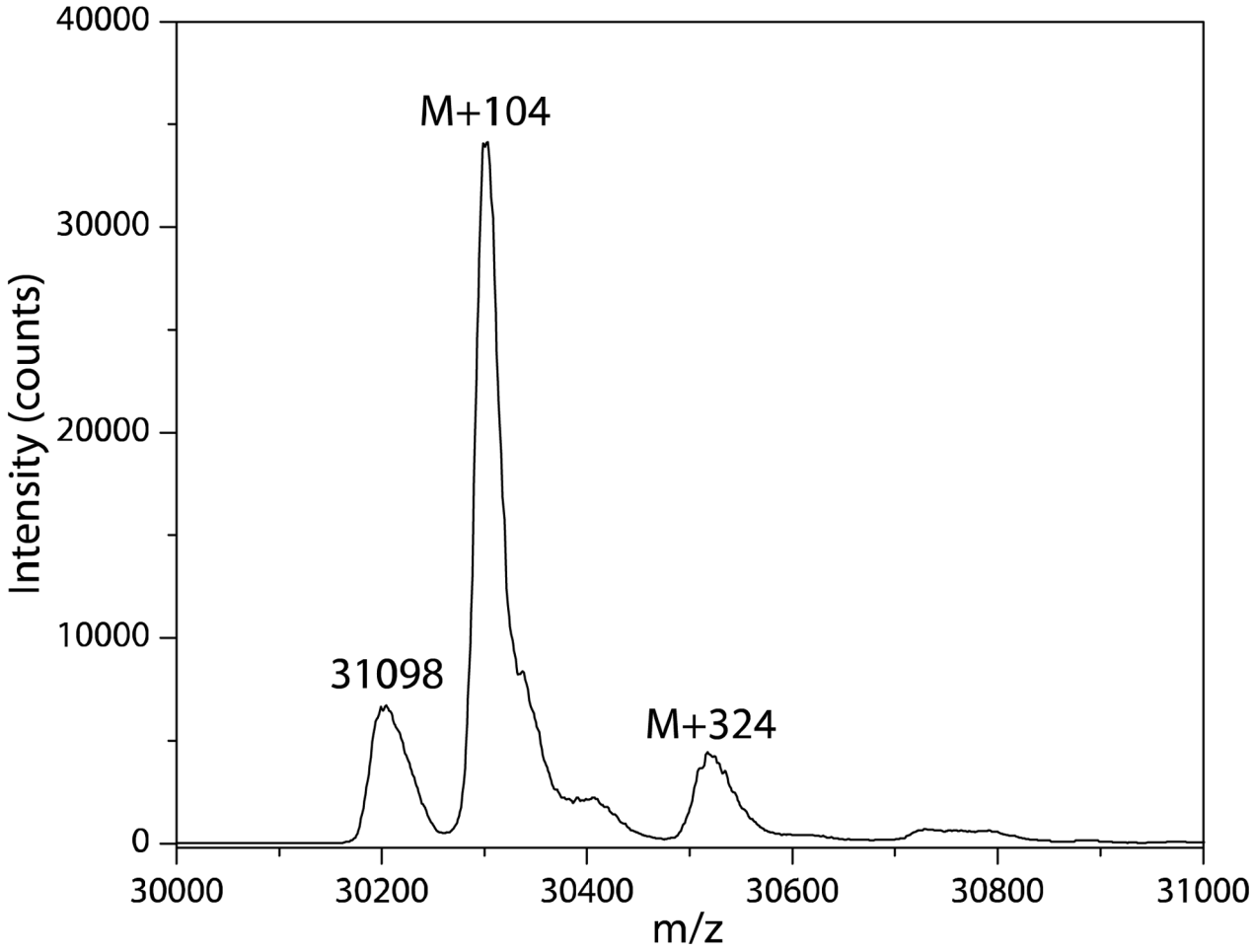

Figure 2.
LC ESI/MS analysis of a reaction mixture of DxnB2 with five-fold excess HOPDA, quenched with 5% acetic acid (v/v) after 10 s. The M+104 and M+324 represent acylated species.

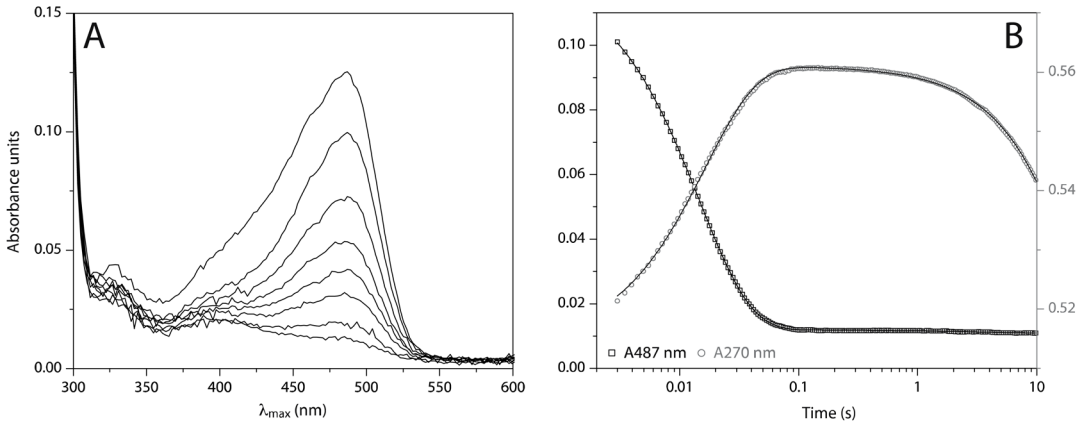

Figure 3.

Results from a representative stopped-flow experiments showing the single turnover of 4 μM HOPDA by 16 μM DxnB2. (A) Reaction monitored using a PDA detector. (B) Reaction monitored at single wavelengths: ES^{red} decay at 487 nm (black) and A270 nm (grey).

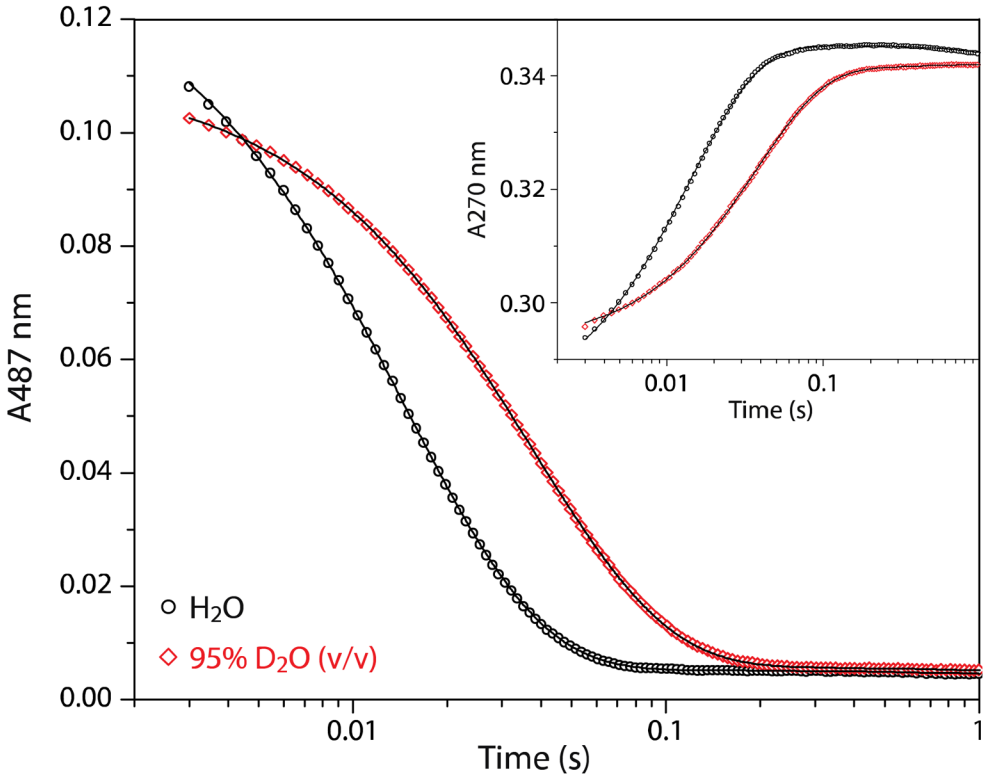

Figure 4.

Results from a representative stopped-flow experiment demonstrating the SKIE on the rate of DxnB2-mediated HOPDA cleavage: ES^{red} decay was monitored at 487 nm in H_2O (black) or 95% D_2O (v/v; red). Data collected at 270 nm are inset.

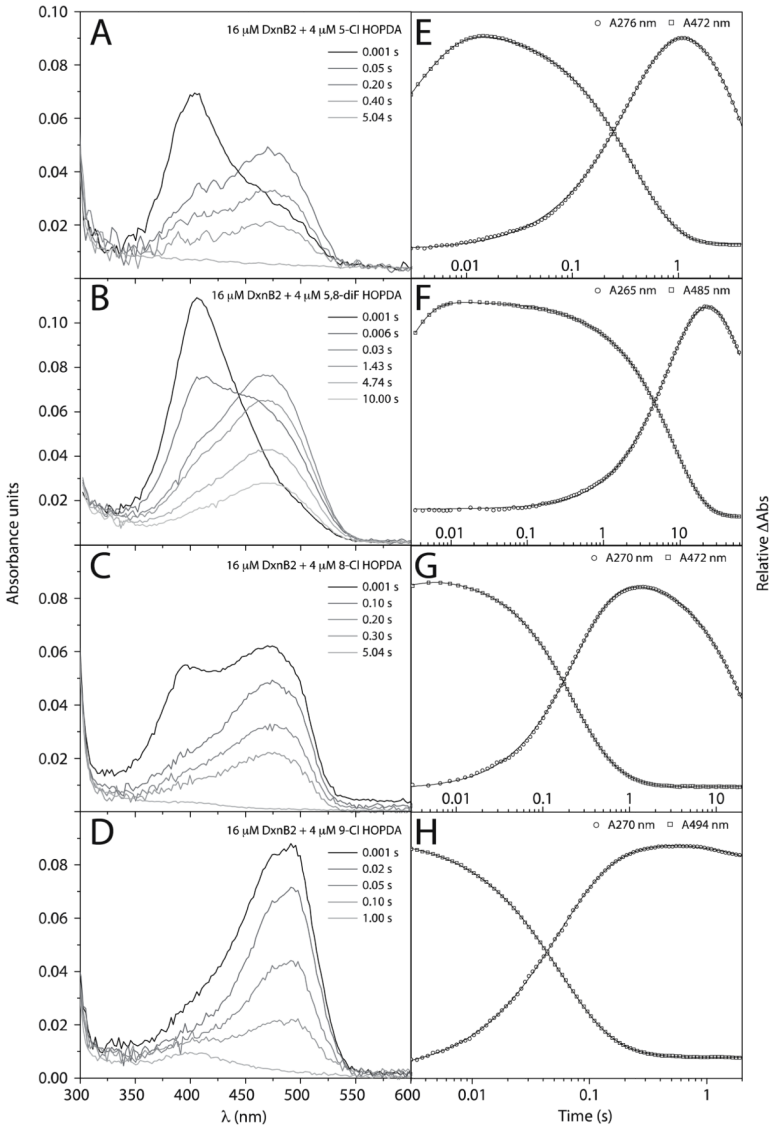

Figure 5.

Results from representative stopped-flow experiments monitoring the turnover of 4 μM substrate by 16 μM DxnB2: (A/E) 5-Cl HOPDA, (B/F) 5,8-diF HOPDA, (C/G) 8-Cl HOPDA and (D/H) 9-Cl HOPDA. The enzymatic and non-enzymatic HPD ketonization can be observed as a decrease in absorbance at 270 nm. The process of HPD rebinding, which accounts for ~1 % of the total change in amplitude is also visible (see Figure S1).

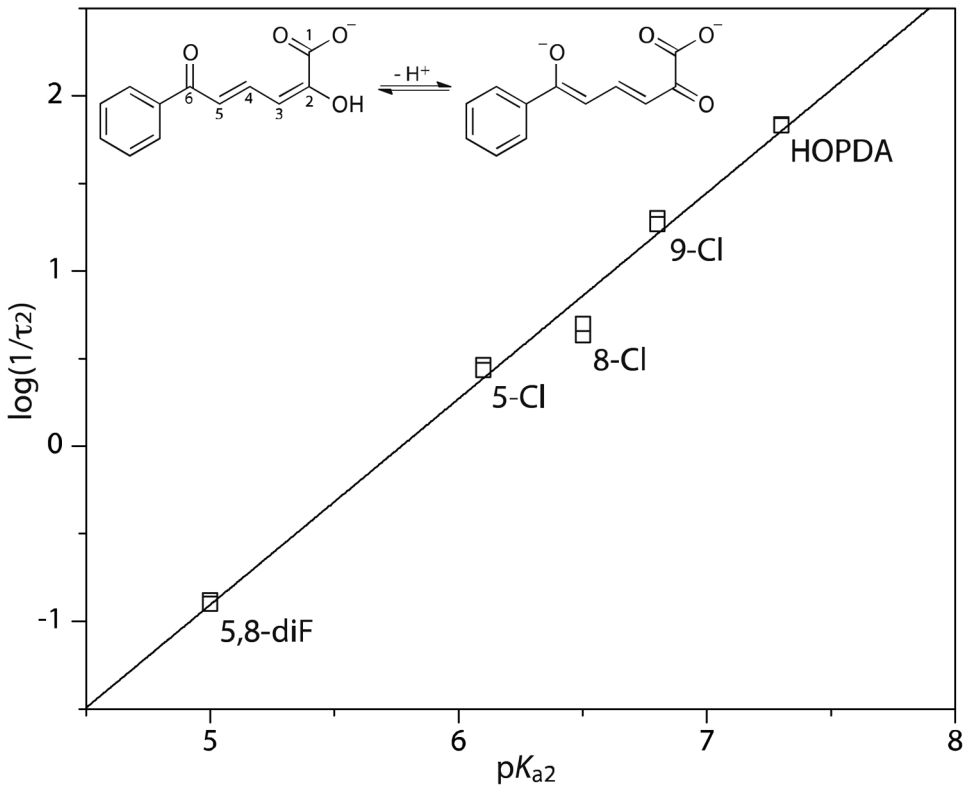

Figure 6.
Extended Brønsted relationship of substrate basicity and the rate of ketonization. The HOPDA enol:enolate equilibrium is inset.

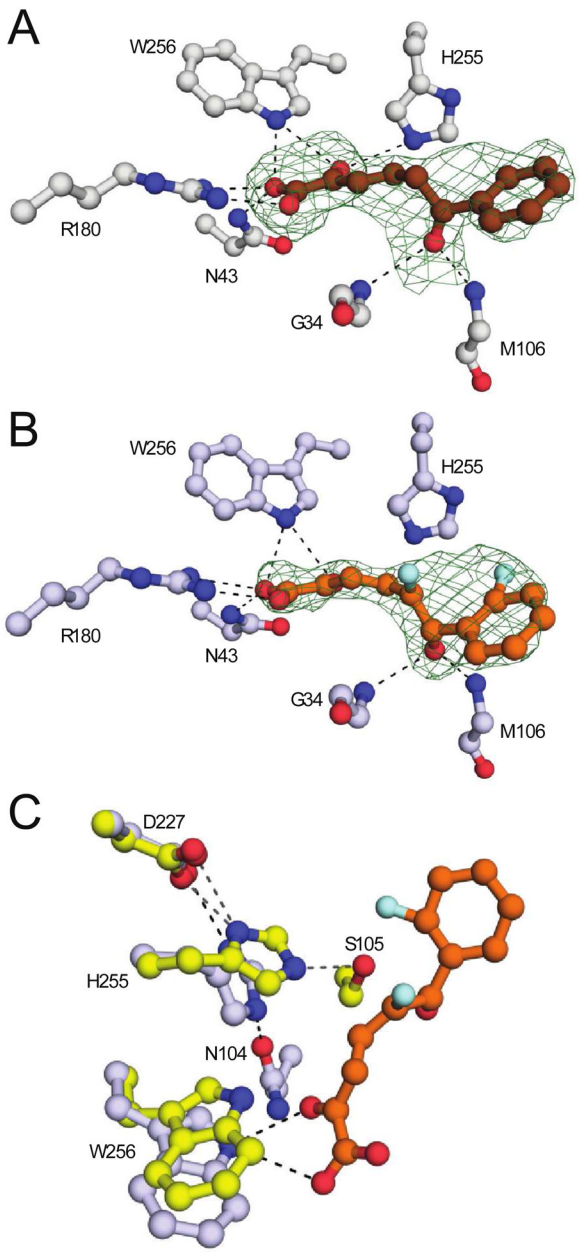

Figure 7.

Ball-and-stick representations of the (A) HOPDA and (B) 5,8-diF HOPDA binding modes to the catalytically inactive DxnB2 S105A variant. The unbiased F_o-F_c maps (green) are shown for each substrate contoured at 3 σ. Relevant polar contacts are drawn as dashed lines (interatomic distances ≤ 3.4 Å). For clarity, the main or side chains atoms of some residues have been removed and some additional polar enzyme-substrate interactions have been omitted. (C) Superposition of DxnB2 WT (yellow) and S105A:5,8-diF HOPDA complex (light blue) active sites showing the concerted movement of His255 and Trp265 upon substrate binding. H-bonding is shown in grey for the WT and black for the binary complex.

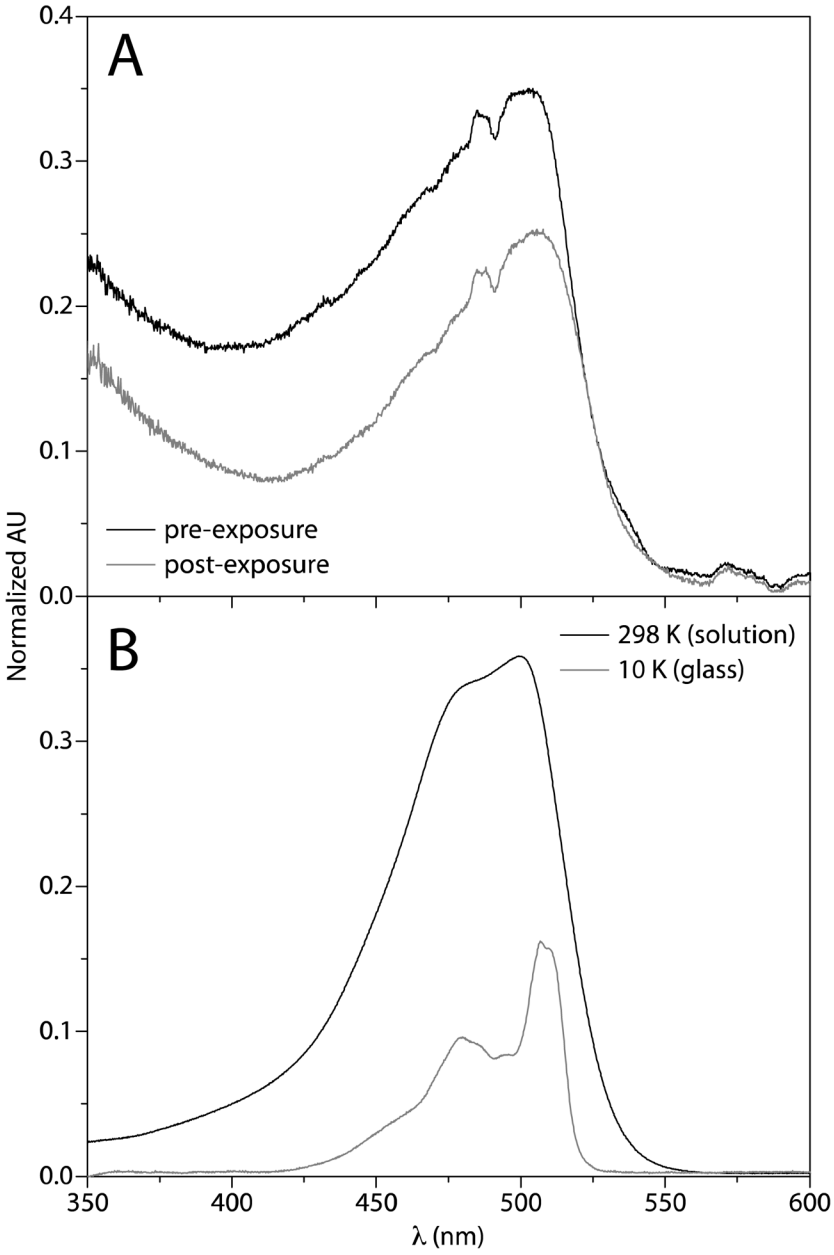

Figure 8.

Electronic absorption spectra of DxnB2 S105A:HOPDA binary complexes. (A) Single crystal absorption spectra pre- (black line) and post-exposure (grey line) to X-rays. (B) The spectra of the S105A:HOPDA complex in a potassium phosphate (I = 0.1 M), pH 7.5 solution at 298 K (25 °C) or frozen as a glass in 50% glycerol at ~10 K.

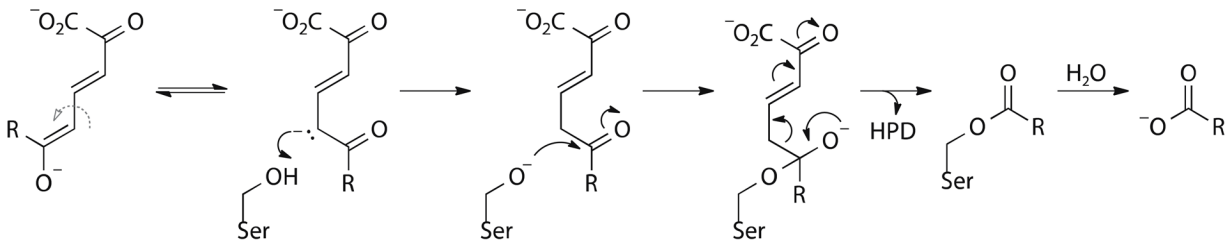

Scheme 1.

The proposed substrate-assisted nucleophilic mechanism of catalysis for the MCP hydrolases, emphasizing substrate ketonization and nucleophile activation. The substrate is drawn as (3*E*, 5*E*)-2-oxo-6-oxido-6-phenylhexa-3,5-dienoate at right due to susceptibility of HOPDA to oxygen exchange into C2 from H_2O[(2)]. The conformation(s) of the predominant HOPDA isomer(s) in aqueous solution are not known. The dashed grey arrow indicates a binding-induced rotation about the C4–C5 bond of the substrate.

Table 1

Pre-steady-state kinetic parameters derived from monitoring HPD formation at 270 nm

[E] (μM)	Substrate	k_{burst} (s^{-1})	Amp_{burst} (ΔA_{270nm})	$[P]_{burst}$ (μM)	v_{ss} (ΔA_{270nm} s^{-1})	k_{ss} (s^{-1})
1	HOPDA	63± 1	0.019± 0.002	1.01± 0.09	0.0079± 0.0002	0.41± 0.01
2.5	HOPDA	61.7± 0.7	0.048± 0.002	2.5± 0.1	0.0173± 0.0009	0.36± 0.02
2.5	9CH	20.0± 0.5	0.032± 0.004	1.67± 0.02	0.208± 0.003	4.34± 0.06

Biochemistry. Author manuscript; available in PMC 2014 October 22.

Table 2

Solvent viscosity and isotope effects on DxnB2-mediated HOPDA hydrolysis[a]

[DxnB2]	λ (nm)	$1/\tau_2$ (s^{-1})
16 μM	270	69 ± 2
	487	68 ± 1
+ 30% sucrose (w/v)	270	67 ± 5
	487	69 ± 1
+ 30% glycerol (v/v)	270	64 ± 5
	487	72.7 ± 0.5
8.2 μM	270	71 ± 2
	487	67.7 ± 0.7
95% D_2O (v/v)	270	28 ± 1
	487	27.0 ± 0.3

[a] For all reactions, ES^{red} was formed within the dead-time of the stopped-flow apparatus: $1/\tau_1 > 500\ s^{-1}$.

Table 3

Kinetic data for the DxnB2-mediated hydrolysis of substituted HOPDAs

Substrate	pK_{a2}[b]	λ (nm)	$1/\tau_1$ (s^{-1}) [% Amp]		$1/\tau_2$ (s^{-1}) [% Amp]		$1/\tau_3$ (s^{-1}) [% Amp]		$1/\tau_4$ (s^{-1}) [% Amp][a]	
HOPDA	7.3	270			69 ± 2	[26 ± 0.2]			0.014 ± 0.001	[74 ± 5]
		487	> 500		68 ± 1	[98.9 ± 0.1]			0.6 ± 0.3	[1.1 ± 0.1]
5-Cl	6.1	270			2.9 ± 0.2	[23.9 ± 0.2]			0.05 ± 0.02	[80 ± 30]
		472	312 ± 5	[43 ± 1]	2.72 ± 0.01					
5,8-diF	5.0	270					0.132 ± 0.002	[20.6 ± 0.3]	0.0018 ± 0.0001	[79 ± 2]
		485	520 ± 20	[46 ± 4]	2.3 ± 0.3	[2.6 ± 0.6]	0.126 ± 0.001	[51.0 ± 0.5]		
8-Cl	6.5	270			4.3 ± 0.1	[43.9 ± 0.6]	1.0 ± 0.2	[52 ± 1]	0.039 ± 0.001	[52 ± 1]
		472	> 500		5.0 ± 0.1	[73 ± 1]	1.76 ± 0.08	[24 ± 1]		
9-Cl	6.8	270			20 ± 1	[52 ± 7]	7 ± 1	[10 ± 5]	0.07 ± 0.02	[40 ± 10]
		494	> 500		18.6 ± 0.5	[91 ± 5]	6 ± 2	[9 ± 4]		
9-Cl HOPDA		270			17.4 ± 0.9	[43 ± 6]	8 ± 3	[6 ± 5]	0.060 ± 0.005	[52 ± 4]
+ 30% sucrose		494	> 500		17.8 ± 0.6	[91 ± 6]	6 ± 3	[8 ± 6]		

[a] $1/\tau_4$ is a measure of post-cleavage processes: HPD rebinding and decay at 487 nm or enzymatic and non-enzymatic HPD ketonization at 270 nm. The considerable uncertainty in these measurements (reflected in the standard deviation between measurements) arises in part because the experiments were designed primarily to investigate the pre-steady-state catalytic events.

[b] pK_{a2} values for HOPDA, 5-Cl, 8-Cl and 9-Cl HOPDA were taken from reference 18.

Table 4

Properties of the crystals, diffraction data, and refinement statistics

	Crystal properties and diffraction data	
Structure	**S105A:HOPDA**	**S105A:5,8-diF HOPDA**
PDB ID	4LYE	4LXI
Resolution range[a] (Å)	56.9 – 2.3	57.3 – 2.2
Space Group	$P6_522$	$P6_522$
Cell Dimensions (Å)	$a = b = 65.7$, $c = 339.3$	$a = b = 66.2$, $c = 342.2$
Unique reflections	19 907	23 287
Multiplicity[a]	10.7 (10.2)	13.7 (7.1)
Completeness[a] (%)	99.5 (45.9)	97.4 (88.1)
R_{symm}[a](%)	9.0 (45.9)	11.0 (49.2)
Mean[a] I/σ^2	26.8 (4.4)	17.3 (2.5)
	Refinement	
R_{factor}/R_{free}	0.20/0.24	0.20/0.26
Model content (atoms)		
Non-hydrogen atoms	2203	2197
Protein	2118	2108
Precipitant/HOPDA[b]	0/16	1/18
Water oxygens	69	70
Average $B_{factors}$ (Å^2)		
all atoms	43.2	48.4
protein	43.2	48.3
precipitant/HOPDA[b]	0/47.2 (0.8)	61.2/66.8
waters	42.4	47.0
rmsd[c] bond lengths (Å)	0.011	0.013
rmsd[c] bond angles (degrees)	1.4	1.5

[a] Values for the highest resolution bin are reported in parentheses,

[b] Each precipitant/ligand was modeled at full occupancy unless otherwise stated in parentheses,

[c] rsmd = root mean square deviation from restraint targets